Transmitter release at the hair cell ribbon synapse

Elisabeth Glowatzki and Paul A. Fuchs

The Center for Hearing and Balance, Department of Otolaryngology–Head and Neck Surgery, The Johns Hopkins University School of Medicine, Traylor 521, 720 Rutland Avenue, Baltimore, MD 21205-2195

Correspondence should be addressed to E.G. (eglowatz@bme.jhu.edu)

Published online: 22 January 2002, DOI: 10.1038/nn796

Neurotransmitters are released continuously at ribbon synapses in the retina and cochlea. Notably, a single ribbon synapse of inner hair cells provides the entire input to each cochlear afferent fiber. We investigated hair cell transmitter release in the postnatal rat cochlea by recording excitatory postsynaptic currents (EPSCs) from afferent boutons directly abutting the ribbon synapse. EPSCs were carried by rapidly gating AMPA receptors. EPSCs were clustered in time, indicating the possibility of coordinate release. Amplitude distributions of spontaneous EPSCs were highly skewed, peaking at 0.4 nS and ranging up to 20 times larger. Hair cell depolarization increased EPSC frequency up to 150 Hz without altering the amplitude distribution. We propose that the ribbon synapse operates by multivesicular release, possibly to achieve high-frequency transmission.

Hair cells, retinal photoreceptors and bipolar cells release their neurotransmitters tonically, modulating the rate of release as stimulus intensity changes[1]. Small, clear synaptic vesicles cluster around plate-like or spherical electron-dense structures called ribbons at sites of afferent contact. It is thought that the synaptic ribbon serves to accumulate or otherwise promote the release of vesicles at these synapses. In the mammalian cochlea, some 10–30 afferent fibers each form a single bouton-like ending on one inner hail cell (IHC), and most such contacts are served by a single synaptic ribbon[2,3]. This single active zone provides the entire acoustic signal for an afferent fiber, including ongoing spontaneous activity up to 100 Hz, evoked action potentials at maximal rates of 300 Hz and phase locking up to 5 kHz[4].

What are the mechanisms that allow continuous, rapid excitation by the ribbon synapse of the hair cell? Capacitance measurements have shown that hair cells[5–9], like retinal cells[10], can sustain high rates of membrane fusion, possibly corresponding to the release of hundreds of vesicles per ribbon per second. Even a single vesicle's transmitter might activate enough current to depolarize the very small afferent bouton to threshold[11]. Indeed, in a limited number of intracellular recordings from afferent fibers, every synaptic potential did evoke an action potential[12]. Neither the previous afferent recordings nor capacitance measurements have sufficient resolution, however, to determine whether transmitter release from the ribbon synapse is quantized, as predicted by the vesicle hypothesis. It also is not known how release at a single ribbon synapse varies with hair cell membrane potential.

In the present study, we used whole-cell, tight-seal recordings from afferent boutons contacting IHCs to provide high-resolution voltage clamp of excitatory postsynaptic currents (EPSCs) at this ribbon synapse. In contrast to the expectation that only single vesicles might be released, the EPSCs had a wide range of amplitudes, which supports an alternative hypothesis of multivesicular release. In the central nervous system, action potential–evoked multivesicular release occurs at single synapses[13]. At the ribbon synapse, however, apparently multivesicular release from the hair cell can occur spontaneously, under conditions in which membrane potential does not vary. Indeed, when the hair cell membrane was depolarized experimentally, EPSC frequency increased but the skewed amplitude distribution was unchanged. Such behavior does not fit the standard picture of calcium-dependent vesicular fusion; rather, it suggests that the ribbon synapse enables multivesicular release through steps that do not depend on the immediate entry of calcium through voltage-gated channels.

Multivesicular release from the hair cell is not required to initiate action potentials in the afferent fiber—indeed, the smallest EPSCs seen here could depolarize the afferent to threshold. Instead, the ribbon may be specialized for multivesicular release to ensure transmission even at the highest rates of stimulation.

Results

Excitatory postsynaptic currents in afferent fibers

We used whole-cell tight-seal methods to record postsynaptic currents from afferent fibers contacting IHCs in apical turns of 7–13-day rat cochleae (the onset of hearing occurs on day 11–12)[14]. The patch pipette directly contacted the terminal swelling of an afferent fiber at the base of the IHC (**Fig. 1**). Entry into the whole-cell configuration on an afferent bouton was evident from a change in holding or capacitative current in some cases, but more often from the appearance of spontaneous EPSCs (described below). The most common alternative was to establish a whole-cell recording from the IHC itself. These recordings were easily distinguished from those of afferent boutons because the neonatal IHC has a substantial input capacitance (7–9 pF), slow cholinergic synaptic currents[15]and Ca^{2+} action potentials[16], none of which occur in the afferent bouton.

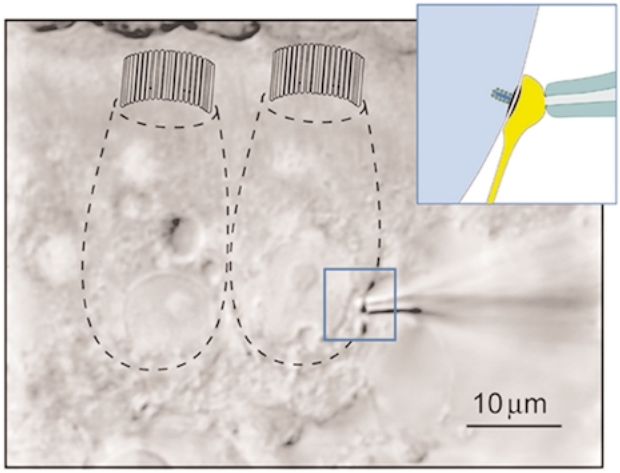

Fig. 1. IHCs contacted by afferent fibers. Two afferent boutons visualized at the base of an IHC by DIC, one with attached pipette tip for whole-cell recording. Inset: most IHC synapses are served by a single synaptic ribbon with clear core vesicles attached (not to scale).

Spontaneous EPSCs were observed in 16 of 21 afferent boutons in saline containing 5.8 mM K^+ (**Fig. 2a**). We elicited EPSCs in silent boutons, or accelerated their spontaneous occurrence by elevating extracellular K^+, thereby depolarizing the IHC and increasing transmitter release onto the afferent fiber (**Fig. 2b**). With some exceptions, EPSCs occurred irregularly, at apparently random intervals. In four boutons studied in 5.8 mM K^+, the average frequency was 1.5 ± 1.1/s (702 EPSCs total). In two additional afferent fibers in 5.8 mM K^+, EPSCs occurred in bursts (**Figs. 7** and **8**). The frequency of EPSCs in 40 mM K^+ was substantially higher: 27.2 ± 22.1/s (n = 5 fibers, 2,950 EPSCs). Application of 1 µM tetrodotoxin (TTX) did not change the frequency, average amplitude or waveform of the EPSCs (**Fig. 2b**), assuring that the postsynaptic activity was not contaminated with unclamped voltage-gated sodium currents from the afferent axon (n = 2).

EPSC amplitudes were markedly variable in all recordings, ranging from 15 to nearly 800 pA in a single bouton. All recordings showed a prominent type of EPSC waveform with a fast rise time and a slower exponential decay (**Fig. 2c**). These monophasic EPSCs represented about 70% of events in all recordings and covered the whole range of EPSC amplitudes. There was some variability in their rise and decay times. In some instances, inflections were visible during the rising phase; these events were counted as monophasic as long as no clear second peak was seen. At a holding potential (V_h) of –94 mV, the mean 10–90% rise time was 0.43 ± 0.10 ms and the mean time constant of decay (τ_{decay}) was 1.07 ± 0.22 ms (mean ± s.d. for 21 boutons, 4,083 EPSCs total; recordings in 5–40 mM K^+ saline). Monophasic EPSCs sometimes appeared as doublets (inset **Fig. 2c**) with intervals up to several milliseconds, and the second EPSC could be larger, smaller or the same size as the first.

In most recordings, a minority of EPSCs (~30%) did not decay with a single exponential. These multiphasic EPSCs had a wide range of waveforms, many seeming to consist of a group of smaller events (left column, **Fig. 2d**). Larger multiphasic events seemed to include a mixture of monophasic EPSCs with smaller components forming inflections on the rising or falling phases (right column, **Fig. 2d**). One interpretation is that multiphasic EPSCs occurred when otherwise simultaneous multivesicular release was dispersed in time.

EPSCs are mediated by AMPA receptors

We recorded EPSCs in 5.8 mM K^+ saline at different holding potentials (**Fig. 3a**) and calculated the mean amplitudes. The resulting current–voltage (I–V) relation was well fit by a straight line passing through 0 ± 11 mV (n = 4) (**Fig. 3b**).

The EPSC time course was voltage dependent, slowing at more positive membrane potentials. In one bouton, for example, the mean τ_{decay} was 0.79 ± 0.14 ms (n = 21) at –94 mV and 1.96 ± 0.38 ms (n = 44) at +56 mV (**Fig. 3a**). Among five boutons, the average ratio of decay time constants at +56 and –94 mV was 2.2 ($p < 0.001$). This voltage-dependent time course

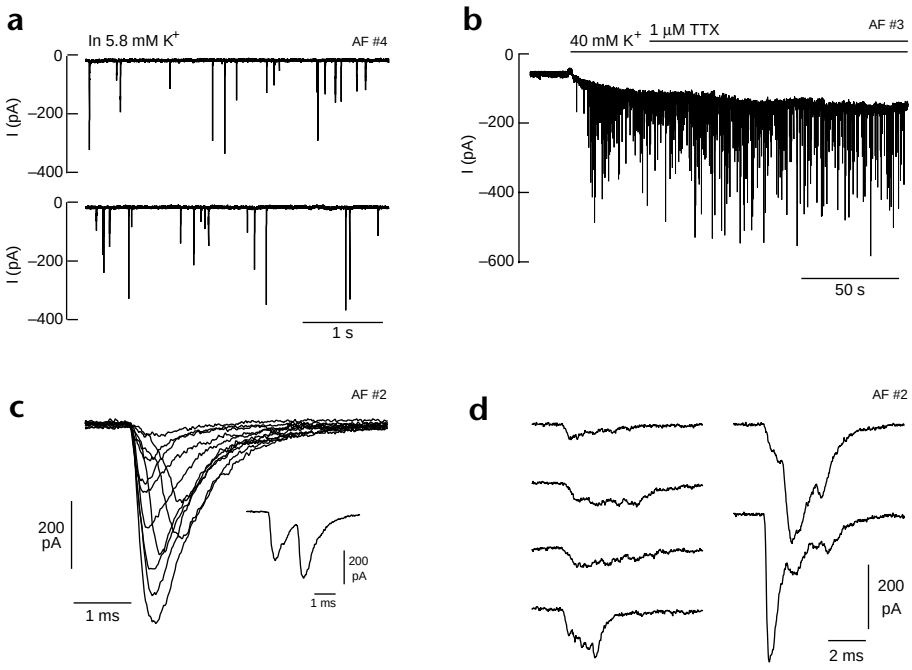

Fig. 2. EPSCs in afferent fibers of IHCs. Whole-cell recordings; holding potential (V_h) –94 mV. (AF #) identifies individual recordings that appear in different figures. (**a**) Afferent fiber in 5.8 mM K^+ saline with irregular 'spontaneous' EPSCs over a wide amplitude range. (**b**) EPSCs activated by application of 40 mM K^+. A steady inward current also was induced by high K^+. One µM TTX had no effect on EPSCs. (**c**) 'Monophasic' EPSCs with fast rise times and a slower exponential decay in 40 mM K^+, aligned at rise time. These represent about 70% of EPSCs in all recordings. Note the slower rise of some intermediate EPSCs. Inset shows double EPSCs observed occasionally. (**d**) 'Multiphasic' EPSCs with a wide range of waveforms, many seeming to consist of a number of events dispersed in time. These represent about 30% of EPSCs in each recording.

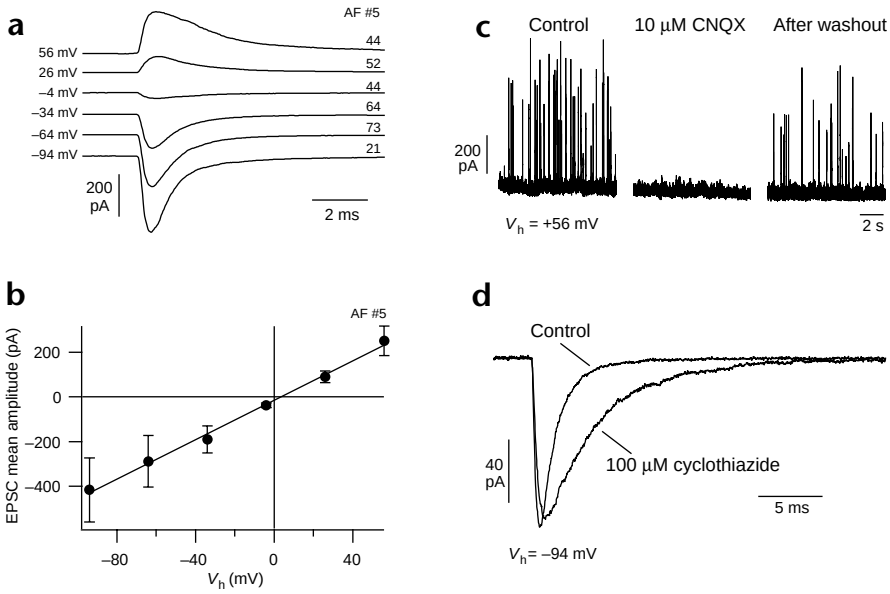

Fig. 3. EPSCs at the IHC ribbon synapse are carried by AMPA receptors. Whole-cell recordings. (**a**) Averaged EPSCs recorded at different membrane potential (V_h) in 5.8 mM K^+ saline. V_h and number of EPSCs per average indicated. EPSC time course slowed at more positive potentials. (**b**) The current voltage relation of the fiber in **a** was non-rectifying and reversed at +3 mV. (**c**) EPSCs at + 56 mV in 20 mM K^+ saline with 2 μM external glycine. 10 μM CNQX completely and reversibly blocked EPSCs. (**d**) EPSCs in 20 mM K^+ saline at –94 mV. Averaged EPSCs in control saline and in 100 μM cyclothiazide. In this fiber, τ_{decay} slowed threefold in cyclothiazide, from 1.22 ± 0.45 ms (n = 25) to 3.62 ± 2.0 ms (n = 20).

has been described before for EPSCs mediated by AMPA receptors[17].

Application of 10–50 μM 6-cyano-7-nitroquinoxaline-2,3-dione (CNQX), an antagonist of AMPA/kainate receptors, completely and reversibly blocked EPSCs at negative (–94 or –84 mV, n = 2) and positive holding potentials (+ 56 mV, n = 3) (**Fig. 3c**). Even at the positive holding potential, intended to relieve the Mg^{2+} block of NMDA receptors, and in the presence of 2 μM glycine as a cofactor for NMDA receptor gating, there were no residual EPSCs when CNQX was present. The tested boutons showed both monophasic and multiphasic EPSCs (**Fig. 2c** and **d**). Thus, all the varieties of synaptic response were sensitive to CNQX.

We also compared EPSC waveforms before and one minute after application of 100 μM cyclothiazide, which reduces the desensitization of AMPA receptors but not kainate receptors[18] (**Fig. 3d**). Cyclothiazide markedly slowed the rate of decay of the EPSCs and had a smaller effect on the rate of rise. In the presence of cyclothiazide, the 10–90% rise time slowed twofold, from 0.42 ± 0.01 ms to 0.96 ± 0.24 ms (n = 3 cells, $p < 0.01$), and τ_{decay} slowed fourfold, from 1.15 ± 0.14 ms to 4.22 ± 0.88 ms (n = 3 cells, $p < 0.001$, 20–186 EPSCs analyzed). We conclude that the EPSCs described here were mediated by AMPA receptors, with no participation of NMDA receptors. The presence of kainate receptors remains to be tested, although considering the effect of cyclothiazide, it seems probable that, if present, their role is minor.

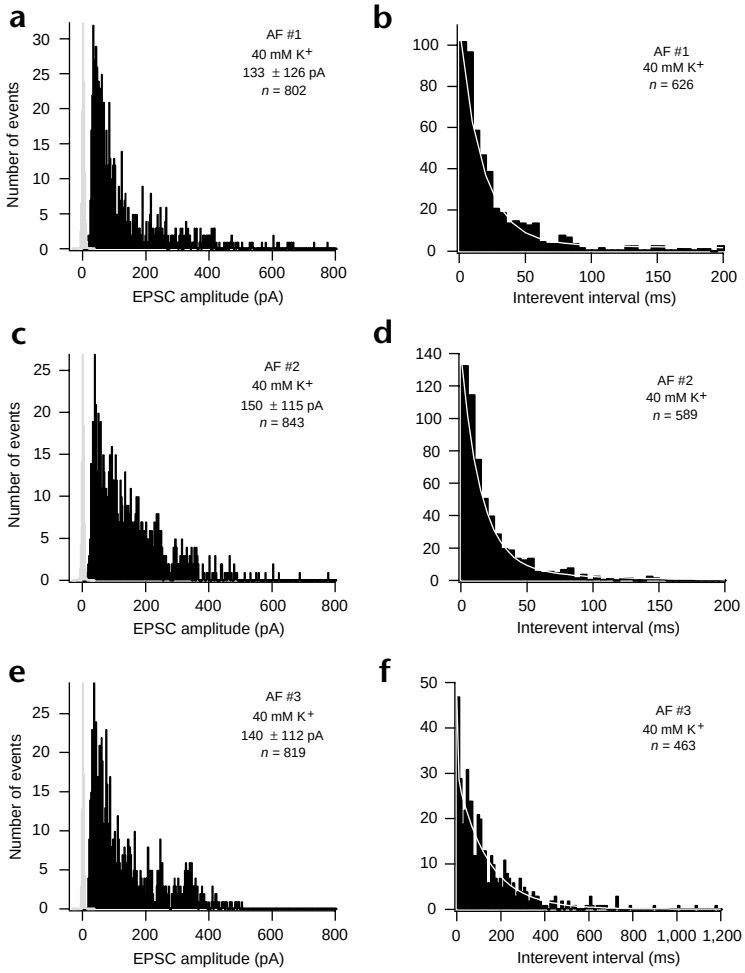

Fig. 4. EPSC amplitude distributions and interevent interval histograms, in 40 mM K^+ saline at –94 mV. (**a**, **c**, **e**) EPSC amplitude distributions were similar in all fibers: highly skewed toward larger amplitudes, with a prominent peak at about 36 pA. All EPSCs, regardless of waveform, were used. Mean amplitudes ± s.d. and numbers of EPSCs (n) are indicated on the histograms; bin width 3 pA. Bars in gray represent the noise of individual recordings, with the maximum of the noise distribution scaled to the maximum of the EPSC amplitude distribution. (**b**, **d**, **f**) Interevent interval histograms were constructed from EPSCs during epochs of relatively constant frequency (bin width 10 ms), with a double exponential fit to the entire interval distribution. The entire histogram is shown for (**f**); only the first 200 ms are shown in **b** and **d**. **b**, τ1 = 18 ms, A1 = 105; τ2 = 250 ms, A2 = 4. **d**, τ1 = 15 ms, A1 = 129; τ2 = 65 ms, A2 = 10. **f**, τ1= 4 ms, A1 = 17; τ2 = 141 ms, A2 = 30.

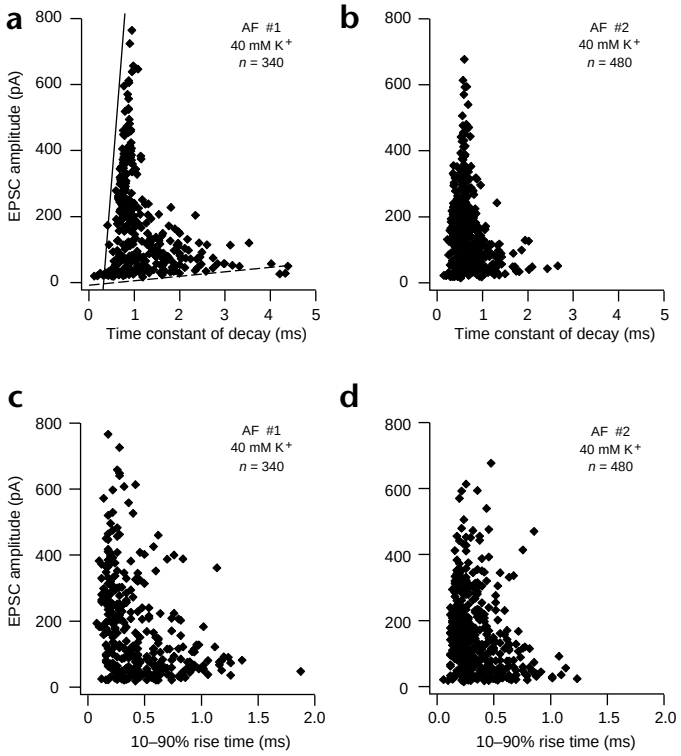

Fig. 5. EPSC amplitude as a function of τ_{decay} and 10–90% rise time, in 40 mM K^+ saline at –94 mV. *n*, number of EPSCs. Only 'monophasic' EPSC amplitudes are included (compare **Fig. 2c**). (**a**, **b**) In each recording, a population of EPSCs with amplitudes >300 pA are closely grouped below the 1 ms τ_{decay}. The fastest τ_{decay} values are seen for the smallest EPSCs. A slight increase in τ_{decay} is seen with bigger EPSCs (solid line in **a**); the dashed line may represent waveforms arising from maximal temporal dispersion of component events. (**c**, **d**) The relation of EPSC amplitude and 10–90% rise time for monophasic EPSCs. Slower rise times include some visibly inflected EPSCs.

Transmitter release during hair cell depolarization

EPSC frequency was markedly increased by application of 40 mM extracellular potassium (**Fig. 2b**). Amplitude histograms were constructed from all EPSCs in each of four fibers (3 shown, **Fig. 4a, c** and **e**). In each case, the amplitude distribution was highly skewed, with a prominent peak at 30–36 pA and a marked extension into amplitudes as much as 20 times larger. The mean amplitudes of the distributions varied between 133 and 171 pA, and the coefficient of variation (CV) was between 77% and 95%.

The mean EPSC frequency in five fibers recorded in 40 mM K^+ was 5, 6, 26, 47 and 52 per second. During the time course of the recordings (lasting between 45 and 218 s), however, the temporal pattern sometimes changed. Application of high-K^+ solution caused a bursting pattern of EPSCs in some cases (**Fig. 7b**), and event frequency fell during some recordings. We therefore used diary plots to choose epochs of relatively constant frequency for interval analysis. The interevent interval histograms were fit with two exponentials: a slower component of 65–250 ms and a faster component of 4–18 ms (**Fig. 4b, d** and **f**). The presence of the faster time constant may reflect the occurrence of 'double EPSCs' and other multipeaked events (**Fig. 2c** and **d**). The multipeaked events could result from a process of multivesicular release whose perfect coordination results in large-amplitude EPSCs but that, when discoordinate, produces the faster time constant. The genesis of the double EPSCs is less certain. The overabundance of short intervals relative to a principal slow time constant, implying a coordinate release process, is still better resolved by analysis of EPSCs in 5 mM K^+ (see **Fig. 6**).

The variation of EPSC waveform with amplitude

Further support for the multivesicular nature of release at the hair cell ribbon synapse can be obtained from analysis of the EPSC waveform. For example, the shape of some multiphasic EPSCs indicated that they may arise from temporal dispersion in the release of multiple vesicles (**Fig. 2d**). Such clearly discoordinate release events could represent one extreme of a continuum that also influences the waveform of the monophasic EPSCs. That is, if large monophasic EPSCs arise from multivesicular release, then the effects of temporal dispersion would reduce the peak amplitude and broaden the overall waveform to prolong the rise and decay times.

To examine this possibility, we plotted the amplitudes of only monophasic EPSCs as a function of τ_{decay} and 10–90% rise time (**Fig. 5a–d**). For four fibers in 40 mM K^+ and nine fibers in

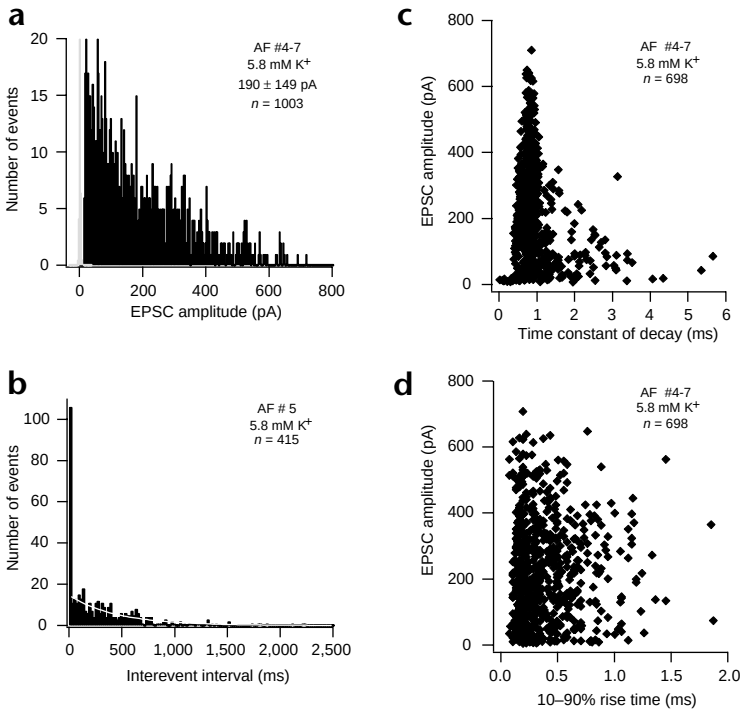

Fig. 6. EPSC analysis in 5.8 mM K^+ saline. V_h –94 mV; mean amplitude ± s.d. indicated; *n*, number of EPSCs. (**a**, **c**, **d**) Data pooled from four recordings with irregular (non-bursting) EPSCs (as in **Fig. 2a**). (**a**) skewed EPSC amplitude distribution with a peak at 18 pA. (**c**, **d**) EPSC amplitudes as a function of τ_{decay} and of 10–90% rise time in 5.8 mM K^+ are similar to those in 40 mM K^+ (see **Fig. 5**). (**b**) Interevent interval histogram of an individual fiber (bin width 20 ms); monoexponential fit with τ at 450 ms (excluding the first bin). The value for the first 20 ms bin (>80% of data points <5 ms) was about 7 times higher than expected from the fit, indicating coordinate release.

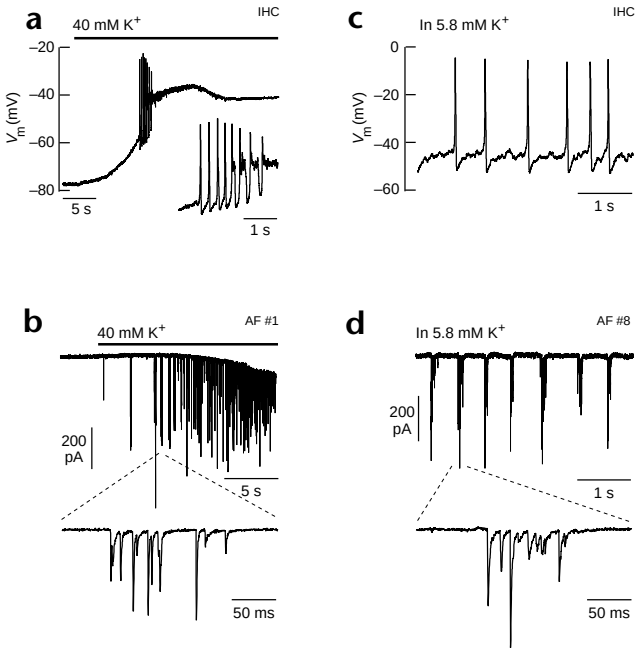

Fig. 7. 'Bursting' activity in postnatal IHCs and afferent fibers, as assessed by whole-cell recordings. (**a**, **c**) Current-clamp recordings from IHCs and (**b**, **d**) voltage-clamp recordings (V_h = –94 mV) from afferent fibers. (**a**) During application of 40 mM K^+, IHCs depolarized, transiently fired Ca^{2+} action potentials (magnified in inset) and then kept a steady depolarized potential. (**b**) During application of 40 mM K^+, EPSCs initially activated in bursts (one burst magnified). (**c**) Action potentials in an IHC in 5.8 mM K^+. (**d**) An afferent fiber showing bursts of EPSCs in 5.8 mM K^+. EPSC bursts occurred at a duration and frequency similar to those of IHC Ca^{2+} action potentials (compare with **c**) and are probably caused by them.

15–25 mM K^+, we saw a uniform pattern in the waveform distribution. The fastest time constants (110–300 μs) were found for the smallest EPSCs, whereas a population of EPSCs with amplitudes greater than 300 pA was grouped closely below the 1-ms τ_{decay} (**Fig. 5a** and **b**). If the smallest EPSCs result from a single vesicle, then a slight increase in decay time (indicated by the solid line in **Fig. 5a**) occurs as more vesicles contribute to make larger EPSCs. On the other hand, if substantial temporal dispersion of multivesicular release were to occur, then smaller, broader EPSCs would be expected, as indicated by the dashed line. Intermediate values of amplitude and time course would result from variable combinations of coordinate and dispersed release events.

As predicted for multivesicular release, the 10–90% rise time shows a pattern similar to that of τ_{decay} when plotted against amplitude (**Fig. 5c** and **d**). The faster rise times span the entire amplitude range, whereas slower rise times correlate with smaller events. The slower rise times presumably include inflected waveforms (**Fig. 2c**). However, the resolution of the very fastest EPSCs may have been obscured by the voltage-clamp time constant, which was estimated to average 40 μs (see Methods). Nonetheless, the general pattern is consistent with the hypothesis that temporal dispersion of multivesicular release broadens the EPSC waveform.

Transmitter release with the hair cell at rest

Having described the features of transmitter release from IHCs when depolarized by 40 mM K^+, we next analyzed release from hair cells with 'normal' resting potentials in 5.8 mM K^+. Because of the low frequency of EPSCs in these conditions, it was necessary to compile data from four recordings to obtain sufficient numbers. The resulting amplitude histogram is highly skewed, with a peak at 18 pA and a broad range of values from 12 to 715 pA (**Fig. 6a**).

The mean amplitude is 190 ± 149 pA, not different from those of fibers recorded in 40 mM K^+. Also, the relation between amplitude and τ_{decay} or 10–90% rise time for monophasic EPSCs in this condition (**Fig. 6c** and **d**) was like that shown for EPSCs in 40 mM K^+ (**Fig. 5a-d**). A column of EPSCs lined up just below a τ_{decay} of 1 msec, with longer decay times spreading to smaller amplitudes. Thus, even though the mean EPSC frequency in 5.8 mM K^+ was 18-fold lower than in 40 mM K^+ (1.5 versus 22.7/s), the amplitude and waveform distributions were similar in the two conditions.

We analyzed interevent interval histograms in two fibers recorded in 5.8 mM K^+. In both cases, short intervals were greatly over-represented. For one fiber, the first bin of the histogram (20 ms width, over 80% of data points <5 ms) was 7 times higher than expected from a monoexponential fit (τ = 450 ms) (**Fig. 6b**), and in a second fiber the first bin (width 50 ms, over 80% < 5 ms) was 4 times higher (τ = 2 s). The excess of short intervals is not predicted by a single stochastic process, but reinforces the notion that multiple release events can be temporally coordinated, consistent with spontaneous multivesicular release.

Ca^{2+} action potentials in IHCs induce EPSC bursting

The data discussed above were obtained without simultaneously recording hair cell membrane potential. Because neonatal IHCs can generate Ca^{2+} action potentials[16], it is possible that some of these EPSCs might represent evoked, rather than spontaneous, transmitter release. Several observations on IHC excitability, however, lead to alternative conclusions. Intracellular recordings from

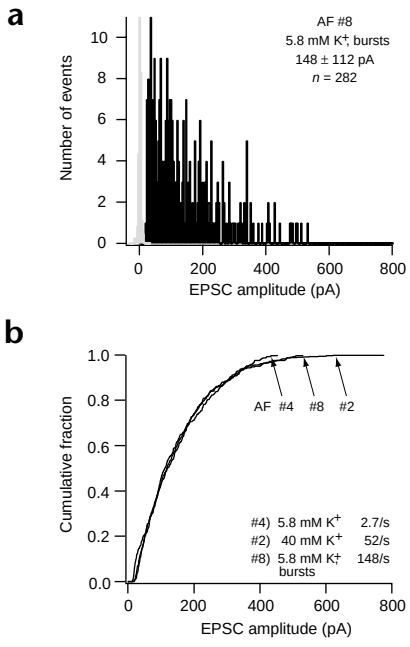

Fig. 8. Comparison of amplitude distributions from afferent fiber recordings with different EPSC frequencies. (**a**) Amplitude distribution of a 'bursting' afferent fiber in 5.8 mM K^+ saline (for original, see **Fig. 7d**). (**b**) Cumulative EPSC amplitude plots for the bursting fiber in **a** and two other afferents recorded in 5.8 or 40 mM K^+ with different EPSC frequencies.

IHCs showed resting membrane potentials between –50 and –75 mV in 5.8 mM K^+ saline. When exposed to 40 mM K^+, the IHCs depolarized to between –40 and –20 mV over the course of several seconds (**Fig. 7a**). In the first seconds of depolarization, IHCs fired a series of Ca^{2+} action potentials before stabilizing at a depolarized voltage. Comparing IHC recordings with recordings from afferent fibers exposed to 40 mM K^+, we saw 'bursts' of EPSCs elicited during the first seconds of 40 mM K^+ application (**Fig. 7b**). EPSC timing then became irregular, as described previously. Occasional IHCs fired repetitive Ca^{2+} action potentials at their resting potential in 5.8 mM K^+, depolarizing to about –10 mV at the peak of the Ca^{2+} action potentials (**Fig. 7c**). During recordings from 2 boutons in 5.8 mM K^+, bursts of EPSCs with corresponding duration and frequency were observed (**Fig. 7d**), presumably resulting from Ca^{2+} action potentials in the presynaptic IHC.

Two points can be made from these observations. First, depolarization with 40 mM K^+ produced Ca^{2+} action potentials in the IHC only in the first few seconds, after which the membrane potential remained stably depolarized at –40 to –20 mV. Thus, EPSCs occurring after the first seconds of K^+ depolarization or in 5.8 mM K^+, when no bursting is seen in the afferent fiber, are spontaneous in the sense that they are not evoked by Ca^{2+} action potentials. Second, the unique pattern of EPSP bursting can be associated with the occurrence of Ca^{2+} action potentials in the IHC, providing thereby an opportunity to examine evoked release from IHCs.

EPSCs vary in frequency but not mean amplitude

The observation of bursting EPSCs presumably activated by IHC Ca^{2+} action potentials (**Fig. 7c**) provides additional insight. Although fewer events were observed, nonetheless the overall shape of the amplitude histogram of a bursting fiber (**Fig. 8a**) is closely related to those seen previously. The mode was at about 30 pA and the mean amplitude was 148 ± 112 pA. These numbers are indistinguishable from those describing spontaneous EPSCs.

From the analysis of EPSCs occurring in different K^+ concentrations and during IHC Ca^{2+} action potentials, it seems likely that amplitude distributions are little altered as release frequency changes. This can be seen more clearly from cumulative probability plots of EPSC amplitudes from three afferent boutons representing a range of conditions and event frequencies (**Fig. 8b**). Irregular, low-frequency (2.7 Hz) EPSCs in 5.8 mM K^+, EPSCs at 52 Hz in a fiber depolarized by 40 mM K^+, and EPSCs occurring at 148 Hz during Ca^{2+} action potential–evoked bursts all had identical distribution functions. Amplitude distributions for these example recordings were unaffected over a more than 50-fold range of release frequencies. This point is also evident by recognizing that four fibers in 40 mM K^+ had EPSC frequencies that varied 10-fold but overlapping cumulative distribution functions (not shown).

Discussion

Intracellular recordings from afferent boutons contacting IHCs provide high-resolution voltage clamping of synaptic currents at this ribbon synapse. The small size of this contact indicates that the observed EPSCs probably arise from single presynaptic active zones, usually comprising one or two synaptic ribbons. Thus, it should be possible to examine the mechanisms of release without the anatomical complexities that hinder analysis at central synapses[13]. An initial goal of our research was to characterize the ligand-gated channels that carry these currents.

Previous work has indicated that neurotransmission at the IHC afferent synapse probably is mediated by AMPA receptors and that NMDA receptors may or may not also be involved[19–22]. Our data here show that EPSCs in afferent fibers contacting postnatal IHCs are mediated by AMPA but not NMDA receptors. We did not look specifically for slower effects that might arise from NMDA receptor gating. AMPA-mediated currents elsewhere in the auditory pathway have rapid gating kinetics[23] and similar properties might be expected at the IHC synapse. The miniature EPSCs (mEPSCs) in bushy cells of the rat AVCN had a τ_{decay} of 350 μs[24] and mEPSCs in the avian nucleus magnocellularis decayed with a time constant of 430 μs[25] (at room temperature). The longer τ_{decay} of 1.07 ms seen in afferent boutons could result from the postulated multivesicular release. Accordingly, the smallest and fastest EPSCs, corresponding perhaps to single quantal responses, had considerably shorter τ_{decay}s, <300 μs.

There is continued speculation as to how ribbon synapses achieve rapid, continuous transmitter release[10]. Is all ribbon release quantized? How does quantal content vary with stimulus intensity? Earlier recordings from vestibular afferents in the frog and goldfish led to the proposition that the ribbon synapse released single vesicles. This was based on the Gaussian distribution of spontaneous synaptic potentials[26,27] (but see more recent disagreement[28]). In contrast, the present study shows that the amplitude of spontaneous EPSCs at the cochlear hair cell synapse is highly variable. We propose that these responses arise not from stochastic release of single vesicles but from coordinate release of varying numbers of vesicles by the ribbon synapse, as has been described for Purkinje cells and single synaptic sites in cerebellar stellate and basket cells[29,30]. This hypothesis is supported by the dual exponential distribution of EPSC intervals, which indicates that a single Poisson process does not describe transmitter release. Indeed, when the average event frequency was below 10 Hz, an excess of very short intervals (<5 ms) was observed. These may reflect the multiphasic EPSCs, which we interpret as imperfectly coordinated, temporally dispersed multivesicular release.

The non-Gaussian EPSC amplitude distributions also are consistent with multivesicular release. These distributions had large CVs (77–95%) and were highly skewed, with the mode at 36 pA, means of 130–190 pA and maxima as high as 775 pA. It seems reasonable to propose that the modal peak represents the quantal size, because the equivalent conductance, 0.40 nS, compares closely to that found in AMPA-dependent synapses in the CNS (0.45 nS)[31]. The average EPSC would then be due to the release of 3–6 vesicles and the largest EPSC would consist of 22 vesicles (assuming linear summation).

How does the distribution of ribbon EPSCs compare to those of other synapses? Some studies on central synapses show that quantal size is well described by single Gaussian functions with low CV (*e.g.*,[32], reviewed recently in[13]), which would accord with the present hypothesis of multivesicular release generating the observed amplitude variability. Other researchers, however, have proposed that variations in vesicle size or contents generate variable quantal sizes, albeit normally distributed and with CVs smaller than those observed here[33,34].

In saccular hair cells of the frog, synaptic vesicle size was normally distributed with a CV (for calculated volumes) of 26% (ref. 35), considerably less than that found here. Variable filling of vesicles cannot be ruled out, but this would imply that fully loaded vesicles occur infrequently and generate quantal responses 20 times larger than those observed in other glutamatergic synapses. Other possible sources of variability include partial activation of receptors due to release at distant sites and incomplete vesicular fusion and release. None of these alternative mechanisms has been tested explicitly here, although a comparison of

the present results to capacitance measurements (see below) indicates that the majority of vesicles probably fuse completely. Whatever the source of variability, it must account for the relationship between amplitude and waveform found in every recording. For example, the entire range of amplitudes occurred among the fastest EPSCs—inconsistent with the predicted effect of distant release sites, which should produce only smaller, slower EPSCs.

Some variability might be attributable to the relative immaturity of these synapses. Hair cell innervation changes progressively during development and may not have been fully mature at the time of our recordings. For example, the contacts of afferent fibers in the gerbil cochlea gradually retract from several to one IHC during the second postnatal week[36]. Distant input from collateral contacts is unlikely to account for EPSC variability, however, as our recordings from a subset of boutons with only short axonal stumps had equally wide amplitude variations.

In addition, during early postnatal development, multiple ribbons are seen in the mouse cochlea, but these are already reduced to one or two per afferent contact in the second postnatal week[37]. Thus, the present recordings could include release from multiple ribbons, perhaps generating some of the observed amplitude variability. If so, vesicular content or postsynaptic receptor density would need to vary widely between immediately adjacent ribbons.

If the ribbon synapse employs multivesicular release, then the amplitude histogram should be described by binomial statistics. We were unable to fit binomial distributions to this data, however. The main problem was that a mean quantum content that could accommodate the initial peak did not predict the larger events. Although there is no verified explanation for the excess of large responses, there is some similarity between this and the distribution of 'large-amplitude miniature inhibitory postsynaptic currents' in cerebellar Purkinje cells[29]. There, the large-amplitude spontaneous currents were attributed to multivesicular release driven by calcium release from intracellular stores. Neonatal IHCs have putative intracellular calcium stores at nearby efferent synaptic contacts that could contribute to such a process[38].

Does a mechanism of multivesicular release fit with other known features of the hair cell ribbon synapse? On the basis of the ultrastructure of the hair cell ribbon, it seems that multiple vesicles could be released simultaneously. Reconstruction of synaptic zones showed that a maximum of 138 vesicles could be closely packed beneath the ribbon (470 nm diameter) in frog saccular hair cells[35]. Extrapolating to the smaller ribbon of the IHC (100×250 nm)[37] yields a maximum of 20 vesicles at close packing, near the present estimates of 22 vesicles for the largest EPSCs.

Capacitance measurements also provide estimates of vesicular release that can be compared to the predicted quantal content of EPSCs. For example, single Ca^{2+} action potentials (duration ~100 ms) in mouse IHCs[5] caused a capacitance increase equivalent to the fusion of 1,000 synaptic vesicles. Assuming 25 synaptic sites per IHC [7], this corresponds to 40 vesicles released per site. During single bursts of EPSCs (mean duration 81 ms) thought to result from IHC Ca^{2+} action potentials, 47 vesicles were released on average (obtained by dividing the summed EPSC amplitudes in a burst by the assumed quantal size). In addition, capacitance measurements have been used to estimate maximum rates of release of ~250 vesicles per second at single synapses of mouse or chicken hair cells[9], verging on the highest rates obtained here (~580 vesicles/s, assuming linear summation of EPSCs in bursts). Although these derivations are subject to numerous uncertainties, the correspondence in the estimated numbers of vesicles provided by different experimental approaches supports the hypothesis that the hair cell ribbon synapse operates by multivesicular release.

Perhaps the most challenging observation made in the present study was that the amplitude distribution of EPSCs did not vary systematically during depolarization that increased release frequency more than 50-fold. It was as though depolarization raised the probability of a 'controlling step' in the release process that then effected the simultaneous release of a variable number of docked vesicles. A related deduction is that the docking of multiple vesicles to make up the readily releasable pool is relatively independent of depolarization and Ca^{2+} influx. The identity of the calcium-dependent controlling step and the mechanism that determines the number of docked vesicles await future experimental testing, but the synaptic ribbon might be involved in both these processes.

What is the functional significance of multivesicular release? An EPSC of 36 pA would cause a 35–70-mV depolarization across the input resistance of the afferent bouton (1–2 GΩ), which makes it likely that single quanta would excite action potentials. Why, then, is there multivesicular release? Perhaps to insure vesicle availability. The hair cell synapse must be able to drive spontaneous and evoked activity in afferent fibers at rates up to several hundred per second. The EPSC frequency in postnatal afferent fibers in 5.8 mM K^+ saline ranged between 0 and 2.7/s. This fits with findings of low spontaneous activity in developing auditory nerve fibers of mammals[39]. The highest EPSC frequencies, however, were found during bursts produced by IHC action potentials, up to 150 Hz. Higher frequencies might occur in mature IHCs where Ca^{2+} influx more efficiently triggers transmitter release[5]. Thus the IHC synapse, even at room temperature, is capable of driving high-frequency afferent activity. In addition, the amplitude distribution of EPSCs was unchanged at the highest rates of release, indicating that the mechanism for recruiting and docking vesicles can operate at still higher frequencies, perhaps to enable phase locking even up to several kilohertz. Thus, continuous and rapid synaptic transmission at the hair cell's ribbon synapse might occur by a mechanism that involves multivesicular release, as suggested in earlier work[12,28]. This mode of operation may be general for ribbon synapses, as large variations in EPSC amplitude also are found in retinal bipolar cells[40].

Methods

Experiments were approved by the Animal Care and Use Committee, Johns Hopkins University. Apical turns of the rat organ of Corti (CD rats, Charles River, Wilmington, Massachusetts) were isolated, mounted under an Axioscope microscope (Zeiss, Oberkochem, Germany) and viewed with differential interference contrast (DIC) using a 63× water-immersion objective and a camera with contrast enhancement (Hamamatsu C2400-07, Hamamatsu City, Japan). The tectorial membrane and cell layers covering the IHCs were taken away using a wide-bore pipette. Currents from afferent fibers were recorded using the whole-cell patch-clamp technique. Methods for patch-clamp recordings from hair cells in this preparation have been established earlier[41]. The pipette solution was 150 mM KCl, 3.5 mM $MgCl_2$, 0.1 mM $CaCl_2$, 5 mM EGTA, 5 mM HEPES buffer, 2.5 mM Na_2ATP, pH 7.2; for some experiments CsCl was substituted for KCl. The extracellular solution was 5.8 mM KCl, 155 mM NaCl, 0.9 mM $MgCl_2$, 1.3 mM $CaCl_2$, 0.7 mM NaH_2PO_4, 5.6 mM glucose, 10 mM HEPES buffer, pH 7.4. Sylgard-coated 1-mm borosilicate glass pipettes had resistances of 15–25 MΩ for bouton recordings and 5–10 MΩ for IHC recordings. Solutions containing elevated potassium or dilute drugs were applied by a gravity-fed multichannel glass pipette (150-μm tip diameter) positioned about 300 μm from the recorded terminal. Currents were recorded with PClamp8 software, with an Axopatch 200B amplifier, lowpass filtered at 5–10 kHz and digitized at 33–50 kHz with a Digidata 1200 board (Axon Instruments, Foster City, California).

Recordings were done at room temperature (22–25°C). Holding potentials were corrected for liquid junction potentials (–4 mV) but not for voltage drop across the uncompensated series resistance (R_s). In most experiments we were not able to compensate R_s because there was no visible change in capacitance when entering whole-cell mode. In these cases, the afferent fiber terminal may have lost its connection to the soma, resulting in a membrane capacitance (C_m) <1 pF. In some afferent fiber recordings with membrane potentials between –42 and –72 mV, we recorded a C_m of 0.5–2 pF and R_s of 29–50 MΩ. Afferent fibers had input resistances of 1–3 GΩ at –94 mV. The clamp time constant was estimated to be less than 40 μs (assuming R_s is 40 MΩ, C_m <1 pF), yielding a bandwidth greater than 4 kHz. The error in EPSC amplitude due to uncompensated R_s would affect only large EPSCs, which represent a small percentage of the data (400–800 pA <5%), and therefore would not affect the calculated *I–V* relations or the peak in the amplitude histograms at 36 pA. For the biggest EPSCs, we estimated the recorded τ_{decay} to be about 120% of the real values due to R_s. As recordings were made directly at the synapse, no distortion due to space clamp is expected. EPSCs were analyzed with Minianalysis (Synaptosoft, Jaejin Software, Leonia, New Jersey). EPSCs were identified using a search routine for event detection with a threshold of 5 pA and confirmed by eye. τ_{decay} values were fit with a monoexponential. Amplitudes of overlapping EPSCs were estimated by fitting the decay of the first EPSC and subtracting the fitted value at the time of the second peak. For further analysis, we used Excel (Microsoft, Redmond, Washington) and Igor Pro (Wavemetrics, Lake Oswego, Oregon). A two-sample *t*-test assuming unequal variances was used for statistical analysis. Data are presented as mean ± s.d.

Acknowledgements

This work was supported by the US National Institute on Deafness and Other Communication Disorders (grant 00276) to P.A.F. We thank A.R. Martin for discussion and data analysis, T.D. Parsons for comments on the manuscript and H. Blum for the design of Figure 1.

RECEIVED 5 SEPTEMBER; ACCEPTED 21 DECEMBER 2001

1. von Gersdorff, H. Synaptic ribbons: versatile signal transducers. *Neuron* **29**, 7–10 (2001).
2. Liberman, M. C. Morphological differences among radial afferent fibers in the cat cochlea: an electron-microscopic study of serial sections. *Hear. Res.* **3**, 45–63 (1980).
3. Liberman, M. C. Single-neuron labeling in the cat auditory nerve. *Science* **216**, 1239–1241 (1982).
4. Johnson, D. H. The relationship between spike rate and synchrony in responses of auditory nerve-fibers to single tones. *J. Am. Stat. Assoc.* **68**, 1115–1122 (1980).
5. Beutner, D. & Moser, T. The presynaptic function of mouse cochlear inner hair cells during development of hearing. *J. Neurosci.* **21**, 4593–4599 (2001).
6. Beutner, D., Voets, T., Neher, E. & Moser, T. Calcium dependence of exocytosis and endocytosis at the cochlear inner hair cell afferent synapse. *Neuron* **29**, 681–690 (2001).
7. Moser, T. & Beutner, D. Kinetics of exocytosis and endocytosis at the cochlear inner hair cell afferent synapse of the mouse. *Proc. Natl. Acad. Sci. USA* **97**, 883–888 (2000).
8. Parsons, T. D., Lenzi, D., Almers, W. & Roberts, W. M. Calcium-triggered exocytosis and endocytosis in an isolated presynaptic cell: capacitance measurements in saccular hair cells. *Neuron* **13**, 875–883 (1994).
9. Spassova, M., Eisen, M. D., Saunders, J. C. & Parsons, T. D. Chick cochlear hair cell exocytosis mediated by dihydropyridine-sensitive calcium channels. *J. Physiol.* **535**, 689–696 (2001).
10. von Gersdorff, H. & Matthews, G. Electrophysiology of synaptic vesicle cycling. *Ann. Rev. Physiol.* **61**, 725–752 (1999).
11. Geisler, C. D. *From Sound to Synapse* Ch. 11, 177–179 (Oxford University Press, New York, 1998).
12. Siegel, J. H. Spontaneous synaptic potentials from afferent terminals in the guinea pig cochlea. *Hear. Res.* **59**, 85–92 (1992).
13. Auger, C. & Marty, A. Quantal currents at single-site central synapses. *J. Physiol.* **526**, 3–11 (2000).
14. Uziel, A., Romand, R. & Marot, M. Development of cochlear potentials in rats. *Audiology* **20**, 89–100 (1981).
15. Glowatzki, E. & Fuchs, P. A. Cholinergic synaptic inhibition of inner hair cells in the neonatal mammalian cochlea. *Science* **288**, 2366–2368 (2000).
16. Kros, C. J., Ruppersberg, J. P. & Rüsch, A. Expression of a potassium conductance in inner hair cells at the onset of hearing in mice. *Nature* **394**, 281–284 (1998).
17. Otis, T. S., Wu, Y.-C. & Trussell, L. O. Delayed clearance of transmitter and the role of glutamate transporters at synapses with multiple release sites. *J. Neurosci.* **16**, 1634–1644 (1996).
18. Partin, K. M., Patneau, D. K., Winters, C. A., Mayer, M. L. & Buonanno, A. Selective modulation of desensitisation at AMPA versus kainate receptors by cyclothiazide and concanavalin A. *Neuron* **11**, 1069–1082 (1993).
19. Nakagawa, T., Komune, S., Uemura, T. & Akaike, N. Excitatory amino acid response in isolated spiral ganglion cells of guinea pig cochlea. *J. Neurophysiol.* **65**, 715–723 (1991).
20. Ruel, J., Chen, C., Pujol, R., Bobbin, R. P. & Puel, J. L. AMPA-preferring glutamate receptors in cochlear physiology of adult guinea-pig. *J. Physiol.* **518**, 667–680 (1999).
21. Ottersen, O. P. *et al.* Molecular organisation of a type of peripheral glutamate synapse: the afferent synapses of hair cells in the inner ear. *Prog. Neurobiol.* **54**, 127–148 (1998).
22. Puel, J. L. Chemical synaptic transmission in the cochlea. *Prog. Neurobiol.* **47**, 449–476 (1995).
23. Trussell, L. O. Synaptic mechanism for coding timing in auditory neurons. *Ann. Rev. Physiol.* **61**, 477–496 (1999).
24. Isaacson, J. S. & Walmsley, B. Amplitude and time course of spontaneous and evoked excitatory postsynaptic currents in bushy cells of the anteroventral cochlear nucleus. *J. Neurophysiol.* **76**, 1566–1571 (1996).
25. Zhang, S. & Trussell, L. O. Voltage clamp analysis of excitatory synaptic transmission in the avian nucleus magnocellularis. *J. Physiol.* **480**, 123–136 (1994).
26. Rossi, M. L., Martini, M., Pelucchi, B. & Fesce, R. Quantal nature of synaptic transmission at the cytoneuronal junction in the frog labyrinth. *J. Physiol.* **478**, 17–35 (1994).
27. Furukawa, T., Hayashida, Y. & Matsuura, S. Quantal analysis of the size of excitatory post-synaptic potentials at synapses between hair cells and afferent nerve fibres in goldfish. *J. Physiol.* **276**, 211–226 (1978).
28. Locke, R., Vautrin, J. & Highstein, S. Miniature EPSPs and sensory encoding in the primary afferents of the vestibular lagena of the toadfish, *Opsanus tau*. *Ann. NY Acad. Sci.* **871**, 35–50 (1999).
29. Llano, I. *et al.* Presynaptic calcium stores underlie large-amplitude miniature IPSCs and spontaneous calcium transients. *Nat. Neurosci.* **3**, 1256–1265 (2000).
30. Auger, C., Kondo, S. & Marty, A. Multivesicular release at single functional synaptic sites in cerebellar stellate and basket cells. *J. Neurosci.* **18**, 4532–4547 (1998).
31. Sahara, Y. & Takahashi, T. Quantal components of the excitatory postsynaptic currents at a rat central auditory synapse. *J. Physiol.* **536**, 189–197 (2001).
32. Forti, L., Bossi, M., Bergamaschi, A., Villa, A. & Malgaroli, A. Loose-patch recordings of single quanta at individual hippocampal synapses. *Nature* **388**, 874–878 (1997).
33. Liu, G. & Tsien, R. W. Properties of synaptic transmission at single hippocampal synaptic boutons. *Nature* **375**, 404–408 (1995).
34. Bekkers, J. M., Richerson, G. B. & Stevens, C. F. Origin of variability in quantal size in cultured hippocampal neurons and hippocampal slices. *Proc. Natl. Acad. Sci. USA* **87**, 5359–5362 (1990).
35. Lenzi, D., Runyeon, J. W., Crum, J., Ellisman, M. H. & Roberts, W. M. Synaptic vesicle populations in saccular hair cells reconstructed by electron tomography. *J. Neurosci.* **19**, 119–132 (1999).
36. Echteler, S. M. Developmental segregation in the afferent projections to mammalian auditory hair cells. *Proc. Natl. Acad. Sci. USA* **89**, 6324–6327 (1992).
37. Sobkowicz, H. M., Rose, J. E., Scott, G. L. & Slapnick, S. M. Ribbon synapses in the developing intact and cultured organ of Corti in the mouse. *J. Neurosci.* **2**, 942–957 (1982).
38. Emmerling, M. R. *et al.* Biochemical and morphological differentiation of acetylcholinesterase-positive efferent fibers in the mouse cochlea. *J. Elect. Micros. Tech.* **15**, 123–143 (1990).
39. Müller, M. The cochlear place–frequency map of the adult and developing mongolian gerbil. *Hear. Res.* **94**, 148–156 (1996).
40. Maple, B. R., Werblin, F. S. & Wu, S. M. Miniature excitatory postsynaptic currents in bipolar cells of the tiger salamander retina. *Vision Res.* **34**, 2357–2362 (1994).
41. Kros, C. J., Rüsch, A. & Richardson, G. P. Mechano-electrical transducer currents in hair cells of the cultured neonatal mouse cochlea. *Proc. R. Soc. Lond. B* **249**, 185–193 (1992).